33RD CONGRESS
OF THE INTERNATIONAL COUNCIL
OF THE AERONAUTICAL SCIENCES
STOCKHOLM, SWEDEN, 4-9 SEPTEMBER, 2022

ICAS 2022 SWEDEN

LQR BASED DIGITAL AUTOPILOT FOR LIGHT SPORT AIRCRAFT

Jan Vlk[1], Peter Chudy[1] & Milan Prustomersky[1]

[1]Faculty of Information Technology, Brno University of Technology, tel: +420541141476, fax: +420541141290

Abstract

This paper addresses research on modern methods in automatic Flight Control System design and evaluation, as seen from the perspective of state-of-the-art and future utilization on Unmanned Aerial Systems. The paper introduces a Flight Control System design process with a special emphasis on the Model-Based Design approach. An integral part of this process is the composition of the aircraft's mathematical model employed in the flight control laws synthesis and the development of a simulation framework for the evaluation of the automatic Flight Control System's stability and performance. The core of this work is aimed at flight control laws synthesis built around the Optimal Control theory. The researched flight control laws originating from the proposed design process were integrated into an experimental digital Flight Control System.

Keywords: aircraft, autopilot, flight control system, Linear Quadratic Regulator, control law synthesis, Model Based Design, stability, performance, digital control

Nomenclature

A_{DS}	[1]	Design system state matrix
A_{IE}	[1]	Integral error model state matrix
A_{PL}	[1]	Plant model state matrix
B_{IE}	[1]	Integral error model input matrix
B_{PL}	[1]	Plant model input matrix
D, L, Q	[N]	Drag, lift and crosswind force
$(\vec{F}_P)_B$	[N]	Propulsion force vector notated in Body-Fixed frame
$\vec{H}^O(t)$	[kg·m^2·s^{-1}]	Angular momentum vector
$\boldsymbol{I}_{BB}$	[kg·m^2]	Inertia tensor in Body-Fixed frame
K_{LQR}	[1]	Linear Quadratic Regulator gain matrix
L_A^G, M_A^G, N_A^G	[N·m]	Aerodynamic moments acting in the center of gravity
m	[kg]	Mass
$\vec{p}(t)$	[kg·m·s^{-1}]	Momentum vector
p, q, r	[rad·s^{-1}]	Angular rates
q_i	[1]	Quaternion elements $i =, 0 \ldots, 3$
$\vec{r}^P$	[1]	Vector of arbitrary point P
u_K, v_K, w_K	[m·s^{-1}]	Kinematic velocity components in Body-Fixed frame
$(\vec{V}_K)_B$	[m·s^{-1}]	Kinematic velocity vector notated in Body-Fixed frame
$(X_A^G)_B, (Y_A^G)_B, (Z_A^G)_B$	[N]	Aerodynamic forces notated in Body-Fixed frame
α, β	[rad]	Angle of attack and sideslip
γ, μ	[rad]	Flight path and bank angle
$\delta_T, \delta_e, \delta_e, \delta_a, \delta_r$	[1]	Throttle, elevator, aileron and rudder deflection
$\zeta_{act}, \omega_{act}$	[1]	Actuator model damping and natural frequency
ϕ, θ, ψ	[rad]	Roll, pitch, yaw angle
$(\vec{\omega}_K^{OB})_B$	[rad·s^{-1}]	Vector of kinematic angular rates notated in Body-Fixed frame

Abbreviations

BFF	Body-Fixed Frame
CG	Center of Gravity
FCS	Flight Control System
LQR	Linear Quadratic Regulator
LSA	Light Sport Aircraft
MBD	Model Based Design
NED	North East Down
RPAS	Remotely Piloted Aircraft Systems
UAS	Unmanned Aerial Systems
UAV	Unmanned Aerial Vehicle

1. Introduction

The market segment of Unmanned Aerial Systems (UAS) experienced a remarkable upturn over the period of last decades. The UAS utilization evolved in a response to emerging new advanced technologies and an associated high demand for application flexibility in serving the surveillance, entertainment industry and cargo transport. Various manned aircraft platforms, which were originally designed for sport and recreational flying, could play an important role in the future UAS development, providing accessible and flexible airframes enabling a cost-efficient holistic design and development. A seamless system integration into the air traffic network places strict demands on operational safety, reliability and robustness of UAS. Addressed elements serve as prerequisites for the future design of advanced automatic flight control techniques in this fast evolving segment. Figure 1 shows the experimental Light Sport Aircraft (LSA), which has been used as a testing platform for the designed digital Flight Control System (FCS).

Figure 1 – Testing platform for Flight Control System Design.

Higher demands on flight endurance and load carrying capacity motivate the conversion of traditionally piloted aircraft to an Unmanned Aerial Vehicle (UAV). However, increased safety requirements have to be considered during such transformation, as well as proper training of the UAV operators. Inexperienced UAV operators with limited flight experience can be ill-prepared for solving critical in flight situations related to bad weather conditions, failures or emergencies, which can suddenly evolve into serious accidents. New technologies aimed at enhanced UAV automation and safety improvements are therefore quickly being introduced to the market. However, these rapidly emerging solutions require thorough testing during the design, development and pre-production stages [1, 2].
This paper introduces the reader to a Model Based Design (MBD) approach in the FCS development, harmonized with the state-of-the-art standards, best practices and regulatory requirements.

2. Light Sport Aircraft Model Dynamics

Before the rigid body nonlinear Equations of Motion (EoM) for an aircraft will be defined, we briefly summarize the assumptions made during the modeling process in the following list [3, 4]:

- Reference point located at the Center of Gravity (CG).
- Rigid body aircraft $\left(\frac{d}{dt}\right)^B (\vec{r}^{RP}) = (\dot{\vec{r}}^{RP})^B$.
- Non-rotating Earth $(\vec{\omega}_K^{IE}) = \vec{0}$.
- Flat Earth $(\vec{\omega}_K^{EO}) = \vec{0}$.
- Quasi-steady aircraft mass $\dot{m} = \frac{dm}{dt} \approx 0$.
- Quasi-steady mass distribution $\left(\frac{d}{dt}\right)^B I^R = 0$.

The previously stated assumptions are valid, as we are addressing a LSA with a fairly limited flight envelope whose dynamics is rather slow as it usually flies at subsonic speeds and small angles of attack. The extensive description of translational and rotational equations of motion can be found in [5, 6, 7, 8].
The translational motion is influenced by different types of forces acting on the aircraft, namely the aerodynamic forces originating from the airflow over the airframe, gravitational forces caused by Earth's gravity and propulsion forces due to the aircraft's propulsion system.
The linear momentum time variation is equal to the sum of all external forces acting on the rigid aircraft, as introduced in equation 1.

$$\frac{d\vec{p}}{dt} = \sum \vec{F} = \frac{d}{dt} \int \dot{\vec{r}}^P(t) \cdot \rho(t) \cdot dV \tag{1}$$

The following equation represents a vector in the Body-Fixed Frame (BFF), rotating at an angular rate ω:

$$\left(\frac{d(\cdot)}{dt}\right)_I = \left(\frac{d(\cdot)}{dt}\right)_B + \vec{\omega} \times (\cdot), \tag{2}$$

where subscripts I and B refer to the Inertial and the BFF, respectively. Equations 3-6 show the translational EoM in a vector format in the BFF,

$$(\dot{\vec{V}}_K)_B = \frac{1}{m} \cdot (\vec{F}_T^G)_B - (\vec{\omega}_K)_B \times (\vec{V}_K)_B, \tag{3}$$

where the variable $(\vec{F}_T^G)_B$ describes the vector of total forces (T) acting in the aircraft center of gravity (G) introduced in the BFF (B) that can be described by the sum of gravitational, aerodynamic and propulsion forces

$$(\vec{F}_T^G)_B = \sum (\vec{F}^G)_B = (\vec{F}_G^G)_B + (\vec{F}_A^G)_B + (\vec{F}_P^G)_B, \tag{4}$$

and the variable $(\vec{V}_K)_B$ is the vector of the aircraft's kinematic velocities (K) expressed in the BFF

$$(\vec{V}_K)_B = [u_K, v_K, w_K]^T \tag{5}$$

The description of the translational motion of an aircraft in BFF coordinate frame is introduced in equation 6.

$$\begin{bmatrix} \dot{u}_K \\ \dot{v}_K \\ \dot{w}_K \end{bmatrix}_B = \frac{1}{m} \begin{bmatrix} X_A^G + X_P^G + X_G^G \\ Y_A^G + Y_P^G + Y_G^G \\ Z_A^G + Z_P^G + Z_G^G \end{bmatrix}_B - \begin{bmatrix} p \\ q \\ r \end{bmatrix}_B \times \begin{bmatrix} u_K \\ v_K \\ w_K \end{bmatrix}_B \tag{6}$$

Equivalently, the translational motion of the aircraft can be described using following parameters, true airspeed V, angle of attack α and angle of sideslip β

$$\begin{aligned}\dot{V} &= -\frac{D}{m}+\frac{(X_P)_B\cos(\alpha)\cos(\beta)}{m}-g\sin(\gamma) &(7)\\ \dot{\alpha} &= -\frac{L}{mV\cos(\beta)}+\frac{-(X_P)_B\sin(\alpha)}{mV\cos(\beta)}+\frac{g}{V\cos(\beta)}\cos(\mu)\cos(\gamma)\\ &+ [q-\tan(\beta)(p\cos(\alpha)+r\sin(\alpha))] &(8)\\ \dot{\beta} &= \frac{Q}{mV}+\frac{-(X_P)_B\cos(\alpha)\sin(\beta)}{mV}\\ &+ \frac{g}{V}\cos(\gamma)\sin(\mu), &(9)\end{aligned}$$

where variables D, L, and Q are the aerodynamic drag, lift and crosswind force and variables γ and μ are the flight path and bank angle, respectively. The resulting rotational motion is generated by the aerodynamic, inertial and propulsion moments acting on the aircraft.
The derivation of the rotational rigid-body EoM is also based on Newton's second law. Let $\vec{H}$ be an angular momentum, then the angular momentum time derivation equals the sum of all external moments acting on the aircraft.

$$\frac{d\vec{H}}{dt}=\sum\vec{M}=\frac{d}{dt}(\vec{r}^P(t)\times\vec{V}^P(t)\cdot m) \tag{10}$$

The angular momentum is simply given by the equation 11.

$$\vec{H}=\boldsymbol{I}\cdot\vec{\omega} \tag{11}$$

Variable $\boldsymbol{I}$ defines the inertia tensor and $\vec{\omega}$ is the angular rate vector.

$$\vec{\omega}=[p,q,r]^T \tag{12}$$

The vector differential that defines the time variation of angular rates is expressed in equation 13,

$$(\dot{\vec{\omega}}_K^{IB})_B^B=(\boldsymbol{I}^G)_{BB}^{-1}\left[\overbrace{\sum(\vec{M}^G)_B}^{External\,moments}\;\overbrace{-(\vec{\omega}_K^{IB})_B\times(\boldsymbol{I}^G)_{BB}(\vec{\omega}_K^{IB})_B}^{Inertia\,cross\,coupling}\right] \tag{13}$$

where $\sum(\vec{M}^G)_B$ is the sum of moments acting in the aircraft's CG and matrix $\boldsymbol{I}_{BB}$ is the aircraft inertia tensor defined by equation 14.

$$I_{BB}=\begin{bmatrix} I_{XX} & -I_{XY} & -I_{XZ}\\ -I_{XY} & I_{YY} & -I_{YZ}\\ -I_{XZ} & -I_{YZ} & I_{ZZ}\end{bmatrix} \tag{14}$$

A detailed form of the momentum equation is shown in equation 15, where the moment vector is expressed as the sum of the aerodynamic and the propulsion part. Since the reference point is assumed to be at the CG, the gravitational force does not contribute to the creation of additional moments around the CG.

$$\begin{bmatrix}\dot{p}\\ \dot{q}\\ \dot{r}\end{bmatrix}_B=I_{BB}^{-1}\begin{bmatrix}L_A^G+L_P^G\\ M_A^G+M_P^G\\ N_A^G+N_P^G\end{bmatrix}_B-\begin{bmatrix}p\\ q\\ r\end{bmatrix}_B\times I_{BB}\begin{bmatrix}p\\ q\\ r\end{bmatrix}_B \tag{15}$$

The vector $\begin{bmatrix}L_A^G & M_A^G & N_A^G\end{bmatrix}^T$ represents aerodynamic moments and vector $\begin{bmatrix}L_P^G & M_P^G & N_P^G\end{bmatrix}^T$ defines the propulsion moments acting around the aircraft's CG. The equation 15 can be rewritten in a

derived form as

$$\begin{aligned}\dot{p} &= \frac{1}{\Delta}\left[I_{zz}L_A^G + I_{xz}N_A^G\right] \\ &+ \frac{1}{\Delta}\left[I_{xz}(I_{xx}-I_{yy}+I_{zz})pq-(I_{zz}^2-I_{zz}I_{yy}+I_{xz}^2)qr\right] \quad (16)\\ \dot{q} &= \frac{1}{I_{yy}}M_A^G+\frac{1}{I_{yy}}\left[I_{xz}(r^2-p^2)-(I_{xx}-I_{zz})pr\right] \quad (17)\\ \dot{r} &= \frac{1}{\Delta}\left[I_{xz}L_A^G + I_{xx}N_A^G\right] \\ &+ \frac{1}{\Delta}\left[(I_{xz}^2-I_{xx}I_{yy}+I_{xx}^2)pq-I_{xz}(I_{xx}-I_{yy}+I_{zz})qr\right], \quad (18)\end{aligned}$$

where the variable Δ is defined by equation 19

$$\Delta = I_{xx}-I_{zz}-I_{xz}^2 \quad (19)$$

The aircraft's attitude in flight is defined using quaternions. This technique has a major advantage over the standard Euler angles stemming from avoiding the manipulation of singularities arising from the aircraft pitch angle reaching the value of $\pm\frac{\pi}{2}$. The attitude differential equations are shown in equation 20.

$$\begin{bmatrix}\dot{q}_0\\ \dot{q}_1\\ \dot{q}_2\\ \dot{q}_3\end{bmatrix} = \frac{1}{2}\begin{bmatrix}0 & -p & -q & -r\\ p & 0 & r & -q\\ q & -r & 0 & p\\ r & q & -p & 0\end{bmatrix}-\begin{bmatrix}q_0\\ q_1\\ q_2\\ q_3\end{bmatrix} \quad (20)$$

A mandatory condition the quaternions must fulfill is its unit normalization introduced in equation 21.

$$q_0^2+q_1^2+q_2^2+q_3^2 = 1 \quad (21)$$

The following functions were employed for the transformation of the quaternions to standard Euler angles that describe the aircraft attitude with respect to the North East Down (NED) frame.

$$\begin{bmatrix}\phi\\ \theta\\ \psi\end{bmatrix} = \begin{bmatrix}\tan^{-1}(2\frac{q_1q_2+q_0q_3}{q_0^2+q_1^2-q_2^2-q_3^2})\\ \sin^{-1}(-2[q_1q_3-q_0q_2])\\ \tan^{-1}(2\frac{q_2q_3+q_0q_1}{q_0^2-q_1^2-q_2^2+q_3^2})\end{bmatrix} \quad (22)$$

For the sake of completeness, we introduce the Euler angles differential equation below.

$$\begin{bmatrix}\dot{\phi}\\ \dot{\theta}\\ \dot{\psi}\end{bmatrix} = \begin{bmatrix}1 & \sin(\phi)\tan(\theta) & \cos(\phi)\tan(\theta)\\ 0 & \cos(\phi) & -\sin(\phi)\\ 0 & \frac{\sin(\phi)}{\cos(\theta)} & \frac{\cos(\phi)}{\cos(\theta)}\end{bmatrix}\begin{bmatrix}p\\ q\\ r\end{bmatrix} \quad (23)$$

2.1 Aircraft State-Space Representation

Equations 24 through 27 introduce the longitudinal motion's state-space model with the state vector x_{lon} and the input vector u_{lon},

$$\dot{x}_{lon} = A_{lon}x_{lon}+B_{lon}u_{lon} \quad (24)$$

$$y_{lon} = C_{lon}x_{lon}, \quad (25)$$

where

$$x_{lon} = [V,\alpha,q,\gamma,h]^T \quad (26)$$

$$u_{lon} = [\delta_T,\delta_e]^T \quad (27)$$

Equations 28 and 29 introduce the internal structures of the longitudinal model's state matrix A_{lon} and the input matrix B_{lon} [9].

$$A_{lon} = \begin{bmatrix} X_V & X_\alpha & X_q & -g\cos(\gamma_0) & X_h \\ Z_V & Z_\alpha & Z_q+1 & -\frac{g}{V_0}\cos(\gamma_0) & Z_h \\ M_V & M_\alpha & M_q & 0 & M_h \\ -Z_V & -Z_\alpha & -Z_q & \frac{g}{V_0}\cos(\gamma_0) & -Z_h \\ \sin(\gamma_0) & 0 & 0 & V_0\cos(\gamma_0) & 0 \end{bmatrix} \tag{28}$$

$$B_{lon} = \begin{bmatrix} X_{\delta_T} & X_{\delta_e} \\ Z_{\delta_T} & Z_{\delta_e} \\ M_{\delta_T} & M_{\delta_e} \\ -Z_{\delta_T} & -Z_{\delta_e} \\ 0 & 0 \end{bmatrix} \tag{29}$$

Variables X, Z, M are respective force and moment coefficients, that are constant for specified trim point condition defined by a combination of velocity and altitude, and are computed during linearization process derived in the previous section. Variables V_0, γ_0 are aircraft states at a trim point. In case of a fully observable state vector, the output matrix C_{lon} from equation 25 is represented by a simple 5×5 identity matrix [10].

The lateral-directional motion model state x_{lat} is composed of flight quantities including sideslip angle β, roll angle ϕ, heading angle ψ, roll rate p and yaw rate r. Input variables of lateral-directional motion are the aileron δ_a and rudder δ_r deflections, which create the input vector u_{lat}. As the derivative of angle of sideslip doesn't have a significant effect on the lateral-directional model dynamics, the related derivatives $Y_{\dot\beta}$, $L_{\dot\beta}$ and $N_{\dot\beta}$ can be neglected. This assumption simplifies the lateral-directional model's system matrix A_{lat} and input matrix B_{lat}.

The following equations define the state-space representation of the lateral-directional dynamics [9].

$$\dot{x}_{lat} = A_{lat}x_{lat} + B_{lat}u_{lat} \tag{30}$$

$$y_{lat} = C_{lat}x_{lat} \tag{31}$$

$$x_{lat} = [\beta, \phi, \psi, p, r]^T \tag{32}$$

$$u_{lat} = [\delta_a, \delta_r]^T \tag{33}$$

Equations 34 and 35 introduce internal structures of the lateral-directional model's state matrix A_{lat} and the input matrix B_{lat}.

$$A_{lat} = \begin{bmatrix} Y_\beta & \frac{g}{V_0}\cos(\alpha_0) & 0 & Y_p+\sin(\alpha_0) & Y_r-\cos(\alpha_0) \\ 0 & 0 & 0 & 1 & \tan(\theta_0) \\ 0 & 0 & 0 & 0 & \frac{1}{\cos\theta_0} \\ L_\beta & 0 & 0 & L_p & L_r \\ N_\beta & 0 & 0 & N_p & N_r \end{bmatrix} \tag{34}$$

$$B_{lat} = \begin{bmatrix} Y_{\delta_a} & Y_{\delta_r} \\ 0 & 0 \\ 0 & 0 \\ L_{\delta_a} & L_{\delta_r} \\ N_{\delta_a} & N_{\delta_r} \end{bmatrix} \tag{35}$$

Variables Y, L, N are, similarly to the longitudinal case, the force and moment coefficients, which are constant for the specified trim point and are computed during the linearization process. Variables V_0, α_0, θ_0 again refer to the aircraft state at the trim point. The output matrix C_{lat} from equation 31 is a 5×5 identity matrix as in the longitudinal motion, which means that all lateral-directional states are assumed to be observable.

2.2 Actuator Model

An important aspect of a digital FCS design is the consideration of the actuator's dynamic effects. The modeled actuator dynamics, with its time delays, influences the aircraft's overall dynamic behavior. The actuator model dynamics can be described by a second order transfer function, with properties expressed in terms of its natural frequency ω_{act} and damping ζ_{act} as shown in the equation (36) [11].

$$F_{act}(s) = \frac{\omega_{act}^2}{s^2 + 2\zeta_{act}\omega_{act}s + \omega_{act}^2} \tag{36}$$

To conveniently combine the actuator model with the state-space representations of the aircraft's longitudinal and lateral-directional motion, the transfer function $F_{act}(s)$ can be transformed into its state-space representation as introduced in equations (37) and (38).

$$\dot{x}_{act} = A_{act}x_{act} + B_{act}u_{act} \tag{37}$$

$$y_{act} = C_{act}x_{act} \tag{38}$$

2.3 Plant Model

The plant model is made of a combination of the aircraft and the actuator state-space model connected via control surface deflections. The output of the plant is a combination of the already defined state vector of the longitudinal or lateral-directional aircraft model and the actuator state as defined by the equation 39

$$x_{pl} = [x_{lat/lon}, x_{act}]^T \tag{39}$$

The plant system for a longitudinal and lateral-directional motion can be defined by equations 40 and 41.

$$\dot{x}_{pl} = \underbrace{\begin{bmatrix} A_{lat/lon} & B_{lat/lon}C_{act} \\ 0^{4\times5} & A_{act} \end{bmatrix}}_{A_{pl}} x_{pl} + \underbrace{\begin{bmatrix} 0^{5\times2} \\ B_{act} \end{bmatrix}}_{B_{pl}} u_{act} \tag{40}$$

$$y_{pl} = \underbrace{\begin{bmatrix} 1 & 0 \end{bmatrix}}_{C_{pl}} \begin{bmatrix} x_{lon/lat} \\ x_{act} \end{bmatrix} \tag{41}$$

3. Linear Quadratic Regulator based Control System Synthesis

Since controlling an aircraft requires command tracking capabilities, e.g., maintaining specified airspeed, altitude or heading, the basic Linear Quadratic Regulator (LQR) algorithm has to be augmented with an Integral Error (IE) dynamics, which guarantees the steady-state error minimization of the controlled variables. The LQR based FCS design requires availability of a linear state-space system. Based on the assumption, that a linearized aircraft model can be decoupled into longitudinal and lateral-directional motion models, the FCS for both models will be researched individually. Figure 2 shows the design scheme for an LQR based FCS. It contains three main subsystems, namely the Plant, which is a combination of the aircraft and actuator dynamics, the state feedback matrix K_{LQR}, and an Integral Error Dynamics.

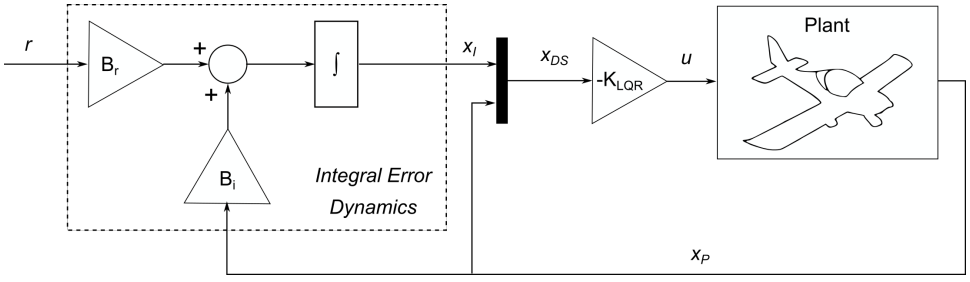

Figure 2 – The LQR system scheme.

The LQR might be employed assuming the full availability of the Design System state x_{DS}, yielding a control law as graphically illustrated in Figure 2.

$$u = -K_{LQR} \cdot x_{DS} \tag{42}$$

At first, the baseline controller for the longitudinal motion model will be expressed. The plant state is defined in the form of the following vector

$$x_{PL_{lon}} = [V, \alpha, q, \gamma, h, \dot{\delta}_T, \delta_T, \dot{\delta}_e, \delta_e]^T, \tag{43}$$

which is a combination of the longitudinal motion model state and the actuator model state. Selected controlled variables in the reference signal r are the commanded airspeed V_{cmd} and altitude h_{cmd}.

$$r = [V_{cmd}, h_{cmd}]^T \tag{44}$$

The IE dynamics state vector x_{IE} contains respective airspeed and altitude errors, as introduced in equation 45.

$$x_{IE} = [e_V, e_h]^T \tag{45}$$

The IE dynamics for the longitudinal motion FCS is described below by the equation 46.

$$\begin{aligned} \overbrace{\begin{bmatrix} \dot{e}_V \\ \dot{e}_h \end{bmatrix}}^{\dot{x}_{IE}} &= \overbrace{\begin{bmatrix} 0 & 0 \\ 0 & 0 \end{bmatrix}}^{A_{IE}} \overbrace{\begin{bmatrix} e_V \\ e_h \end{bmatrix}}^{x_{IE}} + \overbrace{\begin{bmatrix} -1 & 0 & 0 & 0 & 0 & 0 & 0 & 0 & 0 \\ 0 & 0 & 0 & 0 & -1 & 0 & 0 & 0 & 0 \end{bmatrix}}^{B_{IE}} x_{PL_{lon}} \\ &+ \underbrace{\begin{bmatrix} 1 & 0 \\ 0 & 1 \end{bmatrix}}_{B_r} \underbrace{\begin{bmatrix} V_{cmd} \\ h_{cmd} \end{bmatrix}}_{r} \end{aligned} \tag{46}$$

The system for the longitudinal FCS design is a combination of an IE dynamics and a Plant model as show in equation 47.

$$\underbrace{\begin{bmatrix} \dot{x}_{PL_{lon}} \\ \dot{x}_{IE} \end{bmatrix}}_{\dot{x}_{DS}} = \underbrace{\begin{bmatrix} A_{PL_{lon}} & 0^{9\times 2} \\ B_{IE} & A_{IE} \end{bmatrix}}_{A_{DS}} \underbrace{\begin{bmatrix} x_{PL_{lon}} \\ x_{IE} \end{bmatrix}}_{x_{DS}} + \underbrace{\begin{bmatrix} B_{PL_{lon}} \\ 0^{2\times 1} \end{bmatrix}}_{B_{DS}} u + \begin{bmatrix} 0^{9\times 2} \\ B_r \end{bmatrix} r \tag{47}$$

The lateral-directional plant model's state vector is composed of the sideslip β, roll ϕ and heading ψ angle, roll p and yaw r rates, the aileron δ_a and rudder δ_r deflections, and their respective rates as shown in equation 48.

$$x_{PL_{lat}} = [\beta, \phi, \psi, p, r, \dot{\delta}_a, \delta_a, \dot{\delta}_r, \delta_r]^T \tag{48}$$

The controlled variables for the lateral-directional FCS are the sideslip and heading angle commands, which define the content of the reference signal r.

$$x_{IE} = [e_\beta, e_\psi]^T \tag{49}$$

$$r = [\beta_{cmd}, \psi_{cmd}]^T \tag{50}$$

The IE dynamics state vector x_{IE} for the lateral-directional FCS can be expressed using equation 51.

$$\begin{aligned} \overbrace{\begin{bmatrix} \dot{e}_\beta \\ \dot{e}_\psi \end{bmatrix}}^{\dot{x}_{IE}} &= \overbrace{\begin{bmatrix} 0 & 0 \\ 0 & 0 \end{bmatrix}}^{A_{IE}} \overbrace{\begin{bmatrix} e_\beta \\ e_\psi \end{bmatrix}}^{x_{IE}} + \overbrace{\begin{bmatrix} -1 & 0 & 0 & 0 & 0 & 0 & 0 & 0 \\ 0 & 0 & -1 & 0 & 0 & 0 & 0 & 0 \end{bmatrix}}^{B_{IE}} x_{PL_{lat}} \\ &+ \underbrace{\begin{bmatrix} 1 & 0 \\ 0 & 1 \end{bmatrix}}_{B_r} \underbrace{\begin{bmatrix} \beta_{cmd} \\ \psi_{cmd} \end{bmatrix}}_{r} \end{aligned} \tag{51}$$

Similarly to the longitudinal FCS design, the Design System used for the lateral-directional controller can be defined in the form of equation 52.

$$\underbrace{\begin{bmatrix} \dot{x}_{PL_{lat}} \\ \dot{x}_{IE} \end{bmatrix}}_{\dot{x}_{DS}} = \underbrace{\begin{bmatrix} A_{PL_{lat}} & 0^{9\times2} \\ B_{IE} & A_{IE} \end{bmatrix}}_{A_{DS}} \underbrace{\begin{bmatrix} x_{PL_{lat}} \\ x_{IE} \end{bmatrix}}_{x_{DS}} + \underbrace{\begin{bmatrix} B_{PL_{lat}} \\ 0^{2\times1} \end{bmatrix}}_{B_{DS}} u + \begin{bmatrix} 0^{9\times2} \\ B_r \end{bmatrix} r \tag{52}$$

The Design System defined by matrices A_{DS} and B_{DS}, from equations 47 and 47 is used for the computation of the feedback gain matrix K_{LQR}, which is then used for expressing the closed-loop system. The closed system, shown in equation 53, will have an identical structure for the longitudinal and the lateral-directional model.

$$\dot{x}_{cl} = \left(\begin{bmatrix} A_{PL} & 0^{9\times2} \\ B_{IE} & A_{IE} \end{bmatrix} - \begin{bmatrix} B_{PL} \\ 0^{2\times1} \end{bmatrix} K_{LQR} \right) x_{cl} + \begin{bmatrix} 0^{9\times2} \\ B_r \end{bmatrix} r \tag{53}$$

4. Digital Flight Control System Implementation

The rapid prototyping environment MATLAB® / Simulink® was selected for the FCS implementation due to its strong capabilities in control system design and analysis.
The FCS algorithms introduced in foregoing section were at first implemented in the Simulink® environment using its block diagrams. The utilization of the block diagrams instead of the classical programming improves readability, traceability and enables convenient and straightforward modifications of the implemented system, making it useful for rapid prototyping.

4.1 Linear Quadratic Regulator Implementation

The LQR controller implemented in Simulink® environment is shown in Figure 3. The controller structure is based on the algorithm introduced in foregoing section. The reference input vector r is composed of 3 command signals, the airspeed V_{cmd}, altitude h_{cmd} and heading ψ_{cmd}. The controller structure itself contains two main parts, namely the Integral Error Dynamics (used for the command tracking) and feedback gain matrix K_{LQR}. The simulation model also contains the Actuator Saturation, representing actuator's physical limits, Plant Dynamics and Sensor Noise.

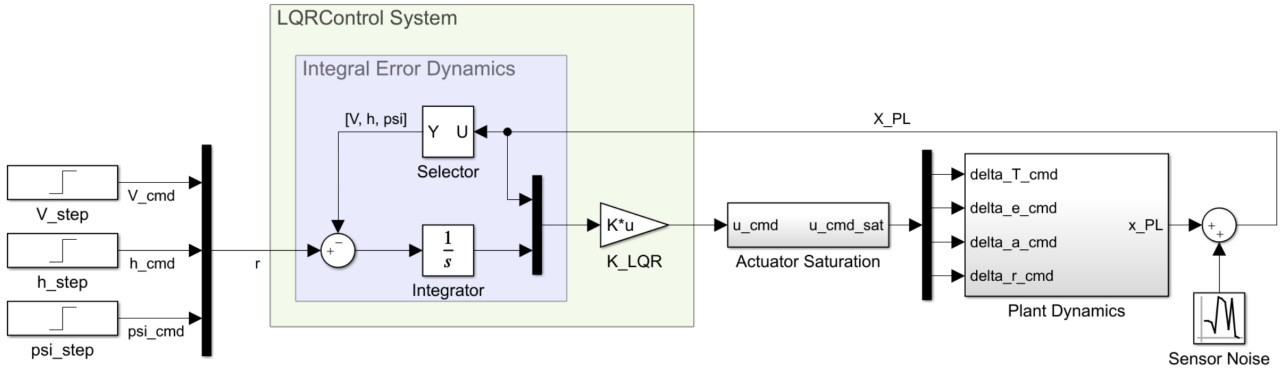

Figure 3 – LQR simulation model implemented in Simulink® .

The Plant Dynamics structure introduced in Figure 4 contains the throttle, elevator, aileron and rudder actuator models connected to the Aircraft Dynamics subsystem in state-space representation. Inputs of the Plant Dynamics subsystems are the commanded control signals generated by the control system. Actuator models process control inputs and generate control deflection and rate signals. Control deflections create the input vector to the Aircraft Dynamics subsystem. The output vector of the Plant Dynamics model x_{PL} is composed of the aircraft states and actuator deflections and rates.
The Actuator Dynamics is modeled using a second-order transfer function. The throttle actuator structure is shown in Figure 5, based on the Actuator Model introduced in Section 2.

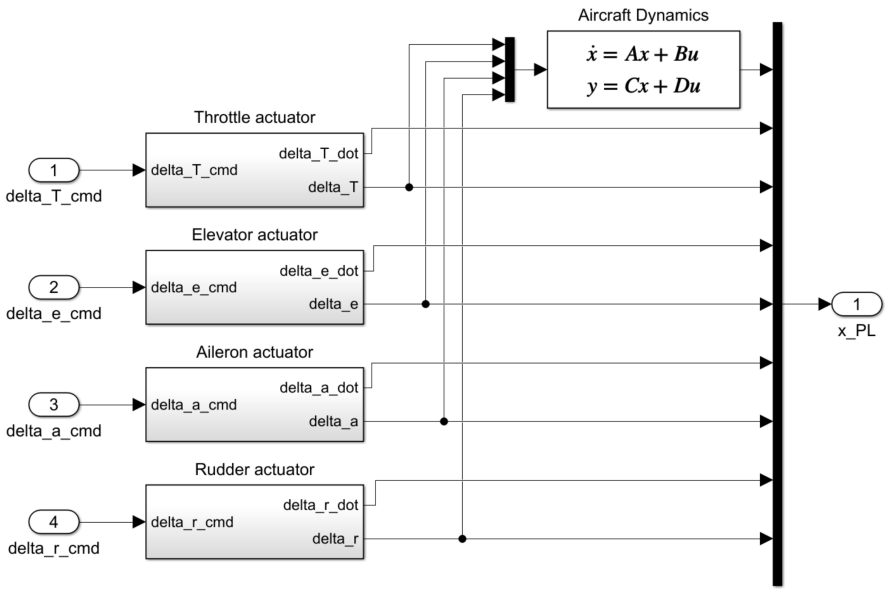

Figure 4 – Plant dynamics structure.

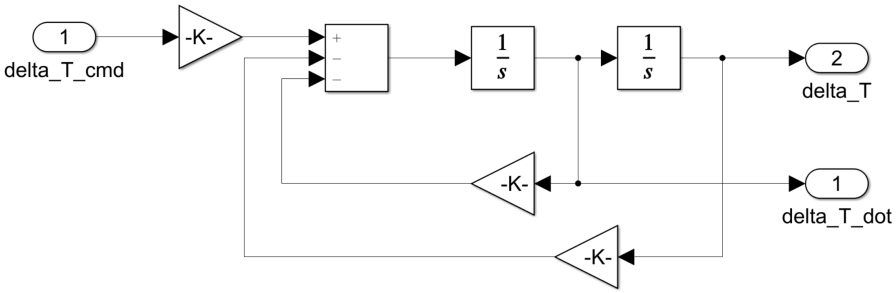

Figure 5 – Actuator dynamics structure.

4.2 Code Generation

The control algorithms implemented using functional blocks in Simulink® can be converted into low-level code like C/C++ directly within the MATLAB® environment. This process is called code generation. The generated code can be integrated into a larger project or compiled through a third-party toolchain, and the executable files can be subsequently deployed to the target hardware. The code generation process is introduced in block diagram in Figure 6 [12].

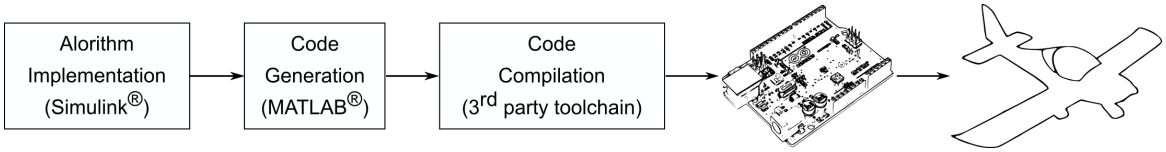

Figure 6 – Code generation and deployment to the target hardware. Source [12]

The FCS implementations details described in the previous subsections were used mainly for the design and evaluation purposes. They contained the modeled aircraft dynamics and were implemented as continuous-time models. However, the model used for the code generation shall be implemented as a discrete-time model and shall contain only the FCS with defined inputs and outputs.
Figure 7 shows the FCS implementation in Simulink® used for code generation with color coded inputs and outputs. The blue input ports are used for the aircraft state measurements while the orange input ports are used as command inputs. The yellow output ports send the computed control surfaces and throttle lever deflection commands to the actuators.

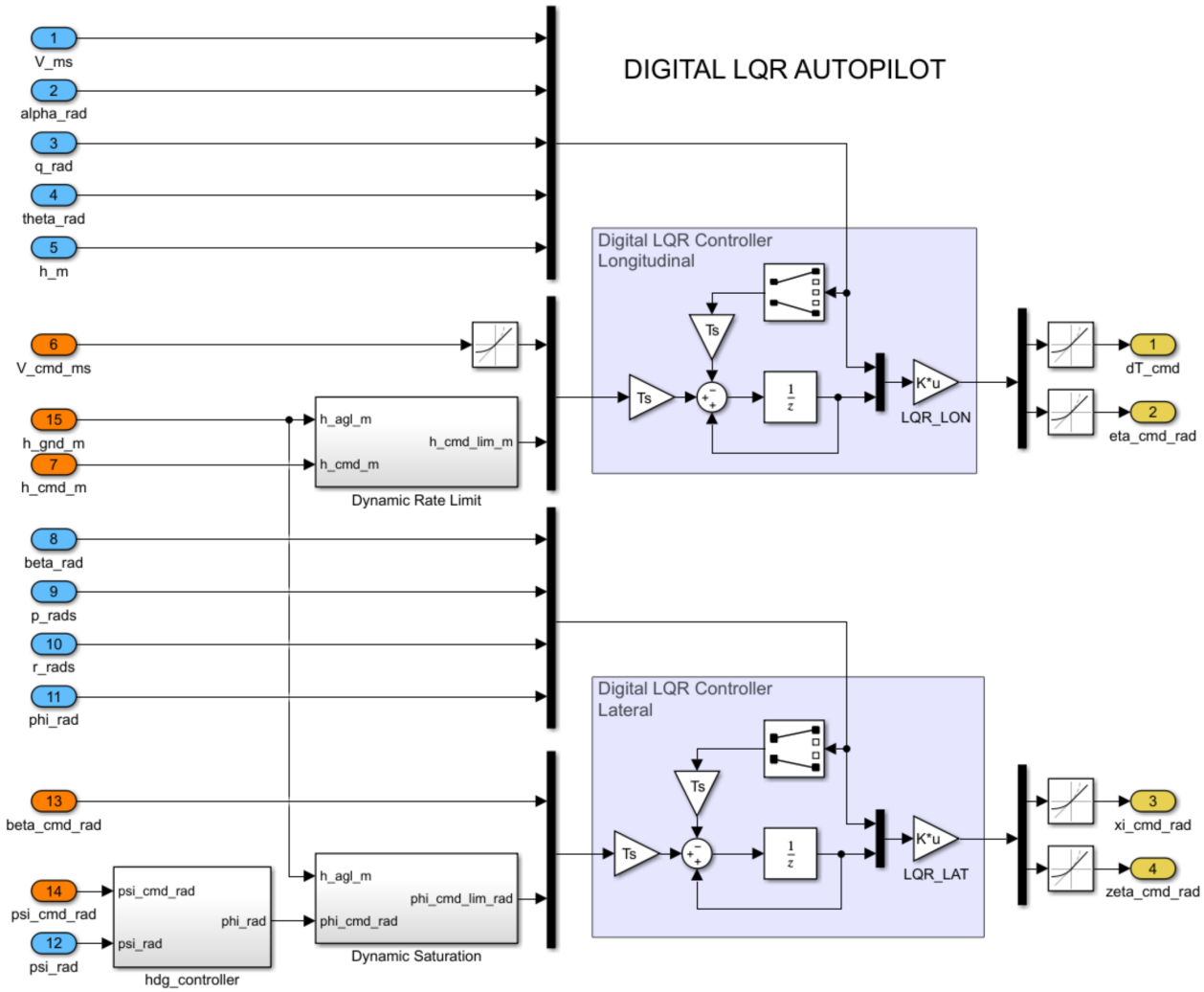

Figure 7 – Simulink® FCS model used for code generation.

5. Flight Test Evaluation

The operational functionality of the FCS algorithms designed for the automatic flight and automated landing approach has been experimentally confirmed in flight experiments performed with an experimental LSA. This section is divided into two subsections. The first subsection describes the automatic flight results with manually inserted command values of altitude, airspeed and heading. The second subsection is focused on a complex task of automatic landing approach.

5.1 Flight Control System Evaluation

An important part of the FCS evaluation is the examination of qualitative indicators of automatic control. The reference SAE-AS94900 [13] was employed in evaluation of the FCS design.

5.1.1 Coordination in Steady Banked Turns

Figure 8 shows the aircraft trajectory in an FCS coordinated turn during practical flight experiments. It also contains the time series of the angle of sideslip β and lateral acceleration a_y. The quantitative limits for this task specified by reference [13] are shown in respective graphs.

- Increment of angle of sideslip β shall not exceed $\pm 2^{\circ}$.
- Lateral acceleration a_y shall not exceed 0.03 g during steady banks.

Based on the evaluation of observed criteria defined by regulation [13] the designed FCS fulfills the above defined requirements.

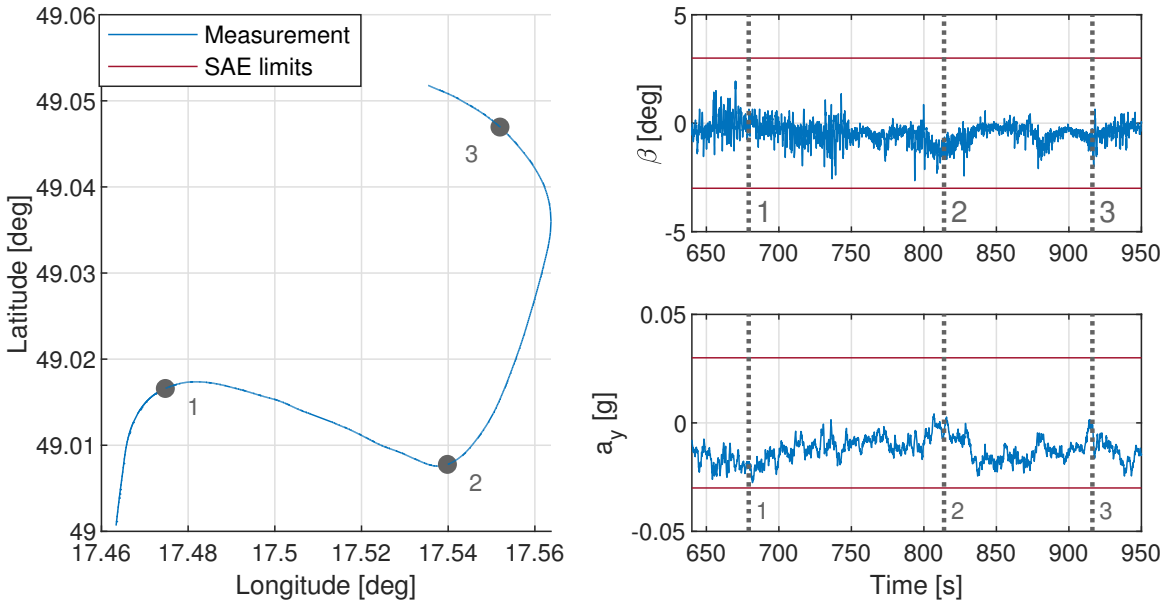

Figure 8 – Coordinated steady banked turns.

5.1.2 Attitude Hold

Figure 9 shows the aircraft trajectory in a steady level flight during the FCS flight test. The aircraft trajectory is augmented by time series of aircraft attitudes described by respective Euler angles, i.e., roll angle ϕ and pitch angle θ measured in steady level flight. Both graphs with measured aircraft attitude contain respective limit values taken from reference [13]. A short list of mentioned criteria is described below:

- For non-turbulent air, the static precision shall be kept within the limits $\pm 0.5^\circ$ for pitch angle and $\pm 1^\circ$ for roll angle with respect to steady-state values.
- In case of a flight in the turbulent atmosphere, the offset in pitch angle shall be lower than 5° RMS, and the offset in roll angle shall not exceed 10° RMS.

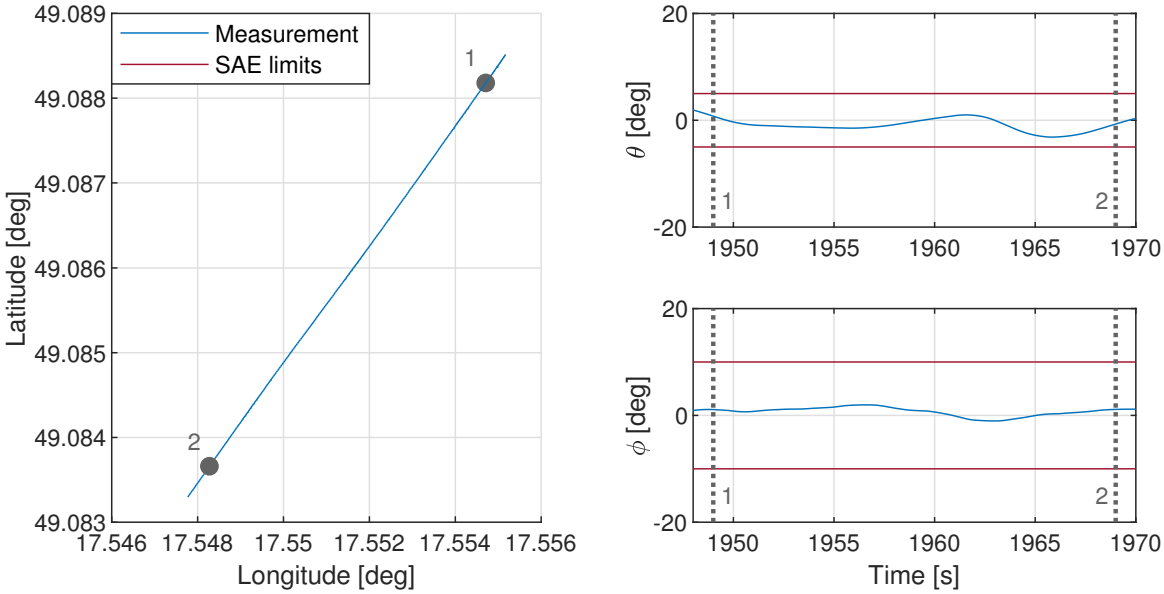

Figure 9 – Attitude hold mode in steady level flight.

Referring to pitch and roll angle measurements in attitude hold mode it can be concluded that the designed autopilot fulfills conditions taken from the reference [13].

5.1.3 Heading Select

Figure 10 shows the aircraft trajectory during a heading change controlled by the FCS as a part of the flight experiment. The figure also contains the aircraft's trajectory during heading change maneuver, commanded and measured heading and measured roll rate p. Both graphs contain limits for control quality evaluations taken from the reference [13]. A short overview of the mentioned criteria is listed below:

- After activation, the FCS shall perform a coordinated turn towards the selected direction with minimal heading change, while maintaining the tolerances mentioned in the subsection Heading Hold.
- The autopilot shall not overshoot the selected heading by more than $1.5°$ in clean configuration and by more than 2.5 ° in configuration with flaps.
- The coordinated turn enter and exit shall be quick and continuous.
- The roll rate p shall not exceed 10 °·s^{-1}.

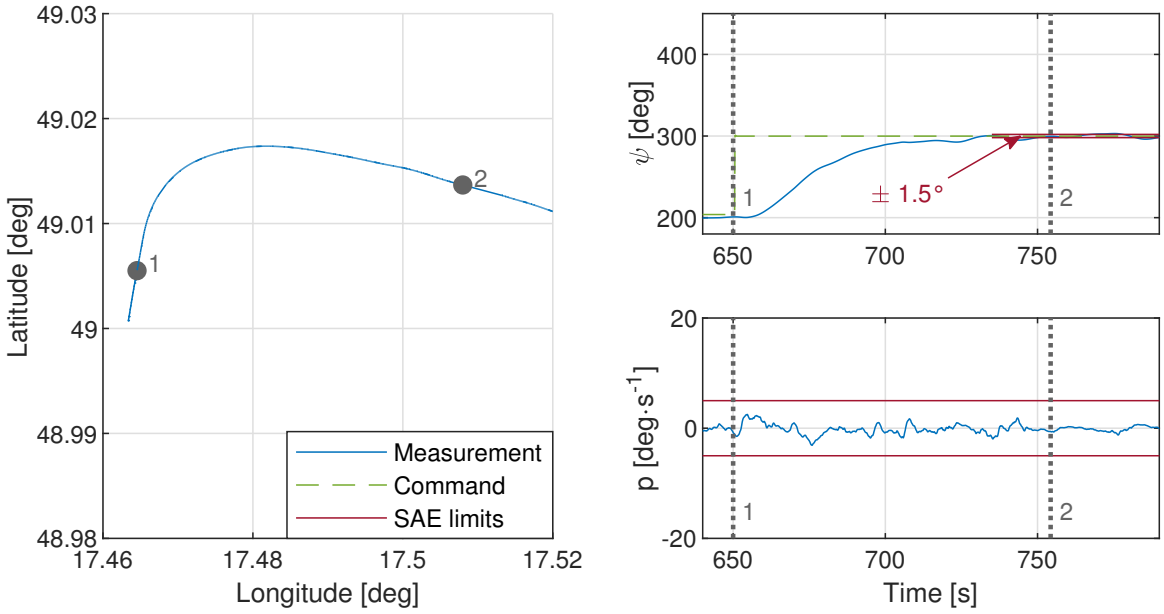

Figure 10 – Heading select mode in level right turn.

Based on the evaluation of monitored criteria defined by reference [13], it can be concluded that the researched FCS fulfills the above defined requirements.

5.1.4 Altitude Select and Hold

Figure 11 shows the aircraft trajectory controlled by the FCS during a flight test. The figure with aircraft trajectory is shown in combination with the time series of aircraft pressure altitude h and normal acceleration a_z. These graphs contain FCS evaluation limits, which were taken from the reference [13]. A short review of the mentioned criteria is listed below:

- For the vertical speed below $\pm 2000\, ft \cdot min^{-}1$, engaging the autopilot shall lead to maintaining current pressure altitude or setting commanded altitude that would be maintained by the autopilot. Acceleration in z-axis shall not exceed $\pm 0.5\, g$.
- Minimal control accuracy for altitude below $30000\, ft$:
  - For roll angle 0 °-1 °, the altitude accuracy shall be within the range $\pm 30\, ft$.
  - For roll angle 1 °-30 °, the altitude accuracy shall be within the range $\pm 60\, ft$ or 0.3%, consider the larger limit.

- After autopilot engage or after any vertical speed instability lower than or equal to $2000\,ft \cdot min^{-}1$, the specified instability shall be recovered until $30\,s$.
- Periodical oscillations shall have a period of at least $20\,s$.

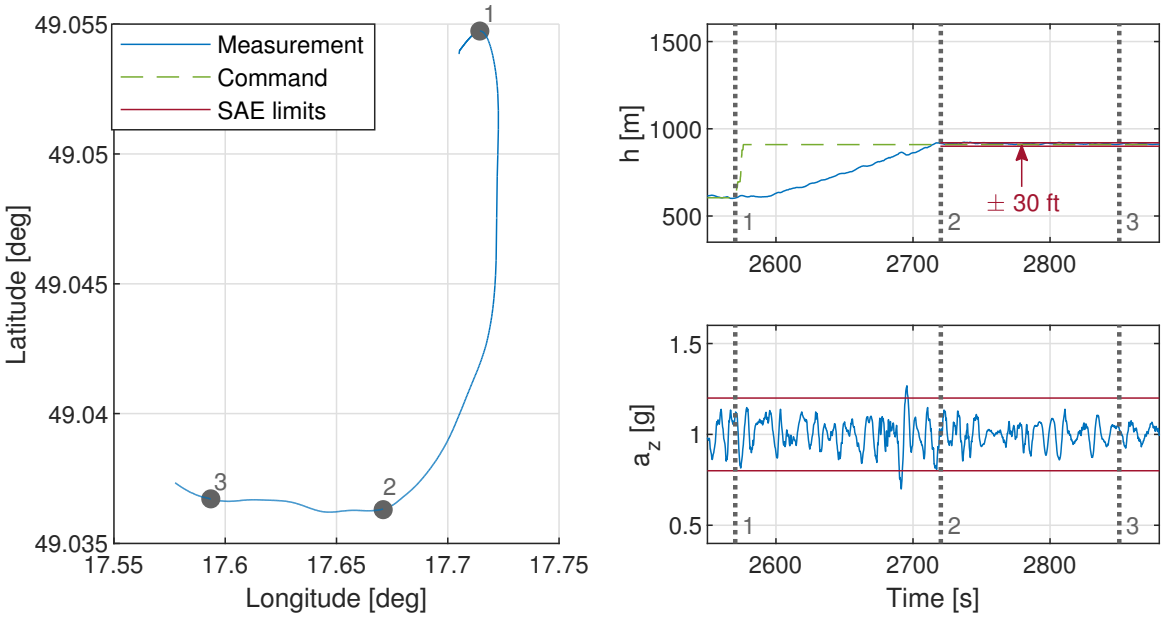

Figure 11 – Altitude select mode.

Based on the evaluation of monitored criteria defined by reference [13], the researched FCS fulfills above defined requirements.

6. Conclusion

This paper demonstrates a modern FCS design, implementation, performance evaluation using flight tests tailored for a fixed-wing LSA. First part of the paper was dedicated to the definition of the aircraft's 6DoF nonlinear model, because precise model and selected structure of the controlled plant, in our case representing an experimental LSA, is essential in designing a well performing FCS. The nonlinear aircraft dynamic model was developed from Newton's laws, in a form of Equations of Motion. The nonlinear system was then linearized to express the aircraft dynamics in a form of a linear state-space model suitable for the FCS research and development, wich was followed by introducing the necessary theory for designing a robust LQR controller and its adjustment to the command tracking task. Implementation of the designed FCS using MATLAB® / Simulink® environment was described next and it introduced the implementation of the designed control system and the low-level code generation for the target hardware platform. The last part of the paper presented the designed FCS's performance evaluations results. The FCS evaluation was focused on the flight experiment results that proved the suitability of the researched FCS.
The future development should account for a higher level of aircraft autonomy. Features as automatic take-off and landing should provide a useful extension to the proposed FCS. The next step could account for a transformation from the experimental LSA platform to RPAS by designing the ground control station with C2 link to the aircraft, taking the pilot out of the flight deck and controlling the aircraft remotely.

Copyright Statement

References

[1] P. Chudy, J. Vlk, and P. Dittrich. Prototyping framework for digital flight control systems. In *2013 IEEE/AIAA 32nd Digital Avionics Systems Conference (DASC)*, pages 7A3–1–7A3–12, 2013.

[2] Robert Goyer. LSA safety picture emerging.

[3] Vladislav Klein and Eugene A. Morelli. *Aircraft System Identification: Theory And Practice*. American Institute of Aeronautics and Astronautics, 2006.

[4] Robert F. Stengel. *Stochastic Optimal Control: Theory and Application*. Wiley-Interscience, 1986.

[5] J.L. Boiffier. *The Dynamics of Flight, The Equations*. The Dynamics of Flight. Wiley, 1998.

[6] Bernard Etkin and Lloyd Duff Reid. *Dynamics of Flight: Stability and Control*. Wiley, 1995.

[7] R.F. Stengel. *Flight Dynamics*. Princeton University Press, 2015.

[8] Jan Roskam. *Airplane Flight Dynamics and Automatic Flight Controls: Part 2*. Darcorporation, 2003.

[9] Brian L. Stevens and Frank L. Lewis. *Aircraft Control and Simulation*. Wiley-Interscience, 2003.

[10] J.P. Hespanha. *Linear Systems Theory*. Princeton University Press, 2009.

[11] Florian Fisch. *Development of a Framework for the Solution of High-Fidelity Trajectory Optimization Problems and Bilevel Optimal Control Problems*. PhD thesis, Technical University of Munich, 2011.

[12] Christoph Hahn. Code generation: Run matlab code and simulink models anywhere!

[13] SAE-International. As94900: General specification for aerospace - flight control systems - design, installation and test of piloted military aircraft. Technical report, 2007.